PORE SCALE MODELING OF WETTABILITY EFFECTS ON WATER-OIL DISPLACEMENT

S.F.R. DA CRUZ†, A. NASCIMENTO‡ and O.J. ROMERO†

† *Graduate Program in Energy, Federal University of Espirito Santo – UFES, São Mateus, ES, Brazil*
‡ *Graduate Program in Chemistry, Federal University of Espirito Santo – UFES, Vitória, ES, Brazil*
suellenfrigatto@gmail.com; andreas.nascimento@ufes.br; oldrich.romero@ufes.br

***Abstract*—– Due to the concern about oil's extraction efficiency decline throughout the time, researchers have looked for alternatives to raise the displacement efficiency of trapped oil within micropores, which has a known complex geometry. The use of numerical simulation presents advantages since it is an economically viable technology with good precision. The current proposition analyzes numerically and with the aid of the Ansys Fluent software, the influence of wettability in microcavity geometry in the displacement of oil by water. Several cases with different radius curvatures of the geometry, contact angles and their influence in displacement efficiency of residual oil are evaluated. The results led to a more realistic analysis regarding the mobilization of trapped oil within the microcavities.**

***Keywords*—– Microcavity; Two-phase flow; Dead-end; Volume of fluid method; Wettability.**

I. INTRODUCTION

The decline of oil production is a great preoccupation in the oil industry (Muggeridge *et al.*, 2014). Although by the time this paper is developed, the world's demand for this energy resource is lower than the offer, which is an atypical situation, the trend is that the increase in consumption will be in a bigger proportion than the production gets to attend. The incorporation of new oil stocks discoveries has reduced, there are a few exceptions to this rule, and the Brazilian pre-salt is an example. The prospection is performed in places with difficult access and sometimes in flora and fauna environments, which should be preserved. The current challenges require, besides new technologies, enormous investments and ways to minimize the environmental impact of the oil prospection and extraction (Pereira *et al*, 2017; Martins *et al*, 2020).

Referring to oil flow during production, one of the most challenging steps is the one involving porous media flow. The reservoir rock, which contains the oil to be produced, can reach up to, or more than a hundred meters underground and has complex access, achievable by drilling techniques. The information that can be obtained from this environment is always involved with uncertainties. The reliability of the collected data improves with time and is very representative when the reservoir must be abandoned, situation in which these data are almost useless.

Besides the presence of uncertainties, mainly when the studies are being performed in order to develop the oil field more efficiently, there are scales ranging from several kilometers to the microscopic scales of some micrometers, in which fluids' typical movement speed is 1 ft/day (1ft = 0.3048 m). This combination of microscale (Fig. 1) and low speed involving immiscible fluids results in a force balance dominated by capillarity force. The viscous forces show its importance when the subject is heavy oils.

The capillarity forces mean the existence of phenomena such as snap off, Jamin effect, strengthening the oil retention. The oil trapping within reservoir rock is one of the main factors leading to the efficiency of the extractive process to be reduced.

Due to economy and practicality, the common way to improve the indexes is to inject water, allowing the oil mobilization. Other alternatives are related to Enhanced Oil Recovery (EOR) methods (Romero and Fejoli, 2015a; Guidi and Romero, 2018; Zitha *et al.*, 2019); however, it requires higher investments and expertise in advanced and expensive technologies. Independent of the technique put in place, an amount of residual oil will remain trapped in the reservoir. It happens because not all the reservoir volume can be contacted by the injected fluid, and at the contacted area not all the oil can be displaced. Therefore, the volumetric efficiency, or macroscopic efficiency, E_V, and the displacement efficiency, or microscopic efficiency, E_D, both are smaller than one.

What does influence the trapping? Is it possible to mobilize trapped oil? How does the mobilization happen? What is the importance of porous geometry in the displacement process? What is the role of properties of the involved fluids? What are the mechanisms involved? The answers to these and other questions are the motivation for the study.

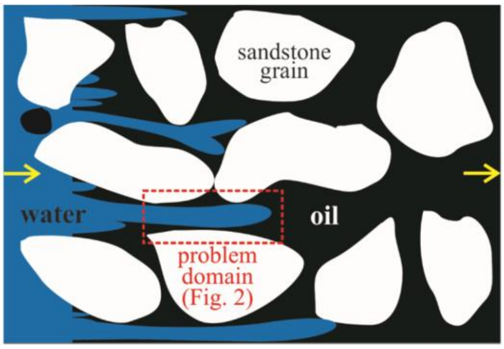

Figure 1. Two-dimensional schematic of porous media where oil is partially displaced by water.

The mobilization of trapped oil in microcavities has been studied since the single-phase perspective (Yin *et al.*, 2006; Kamyabi *et al.*, 2013; Kamyabi *et al.*, 2015) and, more recently, considering as a biphasic flow (Coelho *et al.*, 2016; Rigatto and Romero, 2018; Soares and Romero, 2019).

Yin *et al.* (2006) and Wei *et al*. (2014) studied the flow behavior of a viscoelastic solution of polymers at a microcavity. According to the authors, the numerical results show the viscoelasticity of polymeric solutions as the main factor influencing the displacement efficiency of the oil. Also according to Yin *et al*. (2006), the flow velocity to a viscoelastic solution is higher than to a Newtonian fluid and the viscoelastic nature of polymeric fluids can improve, in general, the oil wettability efficiency in relation to the usage of Newtonian fluids.

Kamyabi *et al*. (2013) and Kamyabi *et al*. (2015) analyzed, numerically, the effects of water injection and of polymeric solutions in the extraction of residual oil. The results obtained show that the viscoelastic fluids have a higher capacity to extract oil of the microcavity. Besides, the results show that the Reynolds number has lower effects in the removal of oil of a microcavity.

The mobilization of trapped oil in a square microcavity was analyzed numerically by Coelho *et al*. (2016), Rigatto and Romero (2018), and Soares and Romero (2019). The authors used the injection of a Newtonian fluid to provide the oil displacement retained in a square microcavity. The results show that only a percentage of the oil is displaced, remaining a large part in the microcavity. The authors also concluded that a higher volume of oil is recovered when the interfacial tension between the fluids is reduced.

Most authors used geometries with corners as a sharp edge to represent the micropores of a reservoir. But, as represented in Fig. 1, this assumption does not correspond to the reality, because corners are not mathematical points and contact lines do not actually pin (Gibbs, 1961; Oliver *et al.*, 1977; Romero *et al.*, 2006).

The current paper proposes to analyze numerically the influence of wettability of water and oil fluids in a pore with rounded corner. Computational techniques are used to evaluate how influence of these values in the displacement efficiency of oil.

II. METHODOLOGY

A. Problem specification

The oil extraction efficiency is quantified by comparing the amount of extracted oil with the initial oil volume contained in the reservoir. This parameter is known as the recovery factor (f_R) that, which is a result of the volumetric efficiency (E_V) multiplied by the displacement efficiency (E_D) (Green and Willhite, 1998), $f_R = E_V E_D$. The volumetric efficiency is obtained considering the reservoir macroscopic scale, and is subject of research of the traditional reservoir simulation. The displacement efficiency refers to the oil mobilization in a microscopic scale.

The current study is directed to phenomena that can be identified mainly on a microscopic scale; therefore,

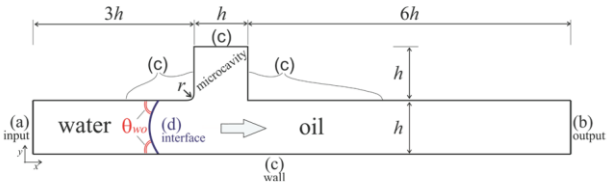

Figure 2. Two-dimensional water-oil displacement in a microchannel with $h = 1$ mm at time t, where three wettability conditions (θ_{wo}) are studied. The letters are boundaries of the domain detailed in section IIB.

the macroscopic efficiency (E_V) is admitted being unitary. The displacement efficiency can be understood as the necessary efforts to mobilize the oil trapped in the rock's porous. Nevertheless, since real problems have complex geometries (Fig.1), simplifications are incorporated in order to make the study viable, resulting in a simplified physical model (Fig. 2), but still preserving the essence and representativeness of the whole. Thus, and as shown in Fig. 2, the geometry is conceived as being formed by two flat and parallel plates, which represent a flat capillary lengthening $10h$ and with a height of h, and with a microcavity square with side h, being h constant and equal to 0.001 m. All geometry is initially filled with oil of viscosity $\mu_o = 10^{-3}$ kg⁄(m s) = 1mPa s = 1cP and density $\rho_o = 900$ kg⁄m^3, in which is injected water of viscosity $\mu_w = 10^{-3}$ kg⁄(m s) and density $\rho_w = 1000$ kg⁄m^3, in the left side of the domain. The fluids are immiscible and the surface tension water-oil is constant valuing $\sigma_{wo} = 7.4 \times 10^{-6}$ N⁄m. The presence of the square cavity and the capillarity and viscous forces are the main drivers of the complex flow of oil displacement.

Because a real porous media is formed by rounded corners, this characteristic has been considered in the simulation. The nearest corner of the entry plane has three values a radius of curvature r equal to 5 mm, 10 mm and 25 mm. In addition, at Fig. 2 it is possible to identify letters that represent the boundary conditions.

The main parameter explored in this paper is the wettability. In a porous media filled with water and oil, the permeability has different behavior if the system is water wetting or oil wetting (Green and Willhite, 1998). The concept of wettability is translated mathematically through the contact angle (θ_{wo} in Fig. 2) between the denser fluid and the wall. Three values for the contact angle are adopted: $\pi/2$ rad, that indicates neutral wettability; π rad indicating the oil as the wetting agent; and 0 rad indicating the water as the wetting agent.

In the two – dimensional configuration of Fig. 2, the injected water volume, $\mathbb{V}_w(t)$ a function of time, invade the volume domain $\mathbb{V}_{total} = 11h^2b$, displacing the fluid contained in this zone, and consequently, the oil volume $\mathbb{V}_o(t)$ reduces with time

The parameter b is the depth perpendicular to the plane. One way to accompany these variations over time t is through the concept of average volumetric fraction $\bar{\alpha}_f(t)$ of fluid f given by Eq. 1, where for water $f = w$ and for oil $f = o$,

$$\bar{\alpha}_f(t) = \mathbb{V}_f(t)/\mathbb{V}_{total}. \tag{1}$$

In the biphasic flow water-oil, the sum of the average of the volumetric fractions at every time instant is a unit, and can be represented as following $\bar{\alpha}_o(t) + \bar{\alpha}_w(t) = 1$.

The information of the oil fraction, which is time-dependent, is particularly important at starting and end of the process. At the beginning ($t = 0$), the oil volume fills the whole domain as following: $\mathbb{V}_f(t = 0) = \mathbb{V}_{o\_inicial} = \mathbb{V}_{total}$. Thus, to the configuration proposed, the average of the volumetric fraction of oil in the beginning phase of the displacement process reaches its maximum value, represented by $\bar{\alpha}_{o\_inicial} = 1$.

As the oil amount reduces, its volume at the end of the injection ($t = t_{final}$) is $\mathbb{V}_{o\_final}$, what represents the oil volume trapped in the microcavity, and consequently, from Eq. 1, the final average oil volumetric fraction is $\bar{\alpha}_{o\_final} = \mathbb{V}_{o\_final}(t)/\mathbb{V}_{total}$.

This parameter represents the oil amount, at fractional terms, that remains trapped within the cavity. As the process is dependent on the water injection time, it is possible to establish the interval of variation of the oil average volumetric fraction, as $\bar{\alpha}_{o\_final} \leq \bar{\alpha}_o(t) \leq 1$.

On the other hand, manipulating previous equations and considering unitary macroscopic efficiency, the oil recovery factor for this physical domain is

$$f_R = 1 - \bar{\alpha}_{o\_final}. \tag{2}$$

From Eq. 2 may be verified that $\bar{\alpha}_{o\_final}$ must have the lower possible value because this reflects how efficient the oil removal process is. As will can be observed during the development this paper, $\bar{\alpha}_{o\_final}$ depends on several dimensionless parameters, like capillarity number (Ca), viscosity ratio (μ_R), contact angle (θ_{wo}), Reynolds number (Re), and of the geometry of the cavity.

Although the equations for $\bar{\alpha}_f$ are presented at average terms to the full domain, they are also valid at any flow point. It means that the volumetric fraction besides time t depends on specific values of the two-dimensional position vector $\mathbf{x} = (x, y)$. Therefore, the representation more appropriate is $\alpha_f(t, \mathbf{x})$, nonetheless to facilitate the following writing, these variables are represented by a simple way only as α_w for water phase and α_o for oil phase.

B. Solution of the immiscible water-oil problem by VOF technique

The presence of the interface, whose form and position, in each domain point and a different instant of time, depends on the operational conditions, liquid properties and geometry, defining the complexity of the displacement process of water-oil, which requires the appliance of specifics numerical techniques aiming to achieve a reasonable solution.

Generally, the methods to address this kind of problems can be classified as (i) moving mesh, and (ii) fixed mesh. The first one requires the solution of additional equations to determine the position of each nodal point, as a response of fluid flow conditions. In the second category, the interface is determined directly, solving also a scalar equation (the mesh is maintained fixed), as is the case of the technique Volume of Fluid – VOF presented by Hirt and Nichols (1981) and used in this paper. In both approaches, additional equations are necessary, which increases the complexity of the problem to be solved. Each method presents advantages and disadvantages. A more detailed explanation of the techniques is out of the scope of this research. Nevertheless, examples of its applications are found at Santos *et al.* (2016) and Coelho *et al.* (2016).

The VOF technique, available in the Ansys Fluent software (Ansys, 2013), was applied to a two-dimensional flow, isothermal, transient, of Newtonian, incompressible and immiscible fluids, and is solved in each point of the domain using the continuity equation, Eq. 3, the momentum equation, Eq. 4, together with the equations that determine the volumetric fractions of each fluid, Eqs. 5 and 6, respectively.

$$\nabla \cdot \mathbf{v} = 0, \tag{3}$$

$$\frac{\partial(\rho_{wo}\mathbf{v})}{\partial t} + \nabla \cdot (\rho_{wo}\mathbf{v}\mathbf{v}) = -\nabla p + \nabla \cdot (2\mu_{wo}\mathbf{D}) + \rho_{wo}\mathbf{g} + \mathbf{f}_{\text{vol}}, \tag{4}$$

where $\mathbf{v}$ is the velocity vector, p is the pressure, $\mathbf{g}$ represents the acceleration of gravity vector, $\mathbf{D}$ the tensor deformation rate defined as $\mathbf{D} = 1/2[\nabla\mathbf{v} + (\nabla\mathbf{v})^{\boldsymbol{T}}]$, being $\nabla\mathbf{v}$ the velocity gradient tensor and the term $(\quad)^{\boldsymbol{T}}$ represents the transposed operation.

The volumetric fraction of the oil phase α_o is determined by

$$\frac{\partial(\alpha_o\rho_o)}{\partial t} + \nabla \cdot (\alpha_o\rho_o\mathbf{v}) = 0, \tag{5}$$

and the water volumetric fraction α_w is obtained directly from

$$\alpha_w = 1 - \alpha_o. \tag{6}$$

Thus, in each point domain of the mesh the volumetric fraction of water α_w and oil α_o can have the following values:

- $\alpha_w = 0$, meaning that it cell does not contains water, only oil ($\alpha_o = 1$);
- $0 < (\alpha_w \text{ or } \alpha_o) < 1$, the cell contains the water-oil interface. In this case, a specific algorithm is used to determine the position and the geometry of the interface inside of each cell;
- $\alpha_w = 1$, when the cell is filled by water, therefore without oil, which means, $\alpha_o = 0$.

Due to the determination of the volumetric fractions to several positions and time instants, and with the specifics mass of water ρ_w and of oil ρ_o as input data, the specific mass ρ_{wo} that covers all regions where the flow of the two fluids occurs is defined as

$$\rho_{wo} = \alpha_w\rho_w + \alpha_o\rho_o, \tag{7}$$

this expression is used to determine the convective term in the Eq. 4. With similar argumentation, the viscosity μ_{wo} is applied in the complete domain and is defined as being

$$\mu_{wo} = \alpha_w\mu_w + \alpha_o\mu_o, \tag{8}$$

that specifies the viscous term of Eq. 4.

Additionally, the term of volumetric fraction $\mathbf{f}_{\text{vol}}$ in Eq. 4 represents the effects of the surface tension σ_{wo}, and is defined by the Continuum Surface Force (CSF) model, presented by Brackbill *et al.* (1992).

$$\mathbf{f}_{\text{vol}} = \sigma_{wo}\kappa\frac{\rho_{wo}\nabla\alpha_o}{1/2(\rho_w+\rho_o)}, \tag{9}$$

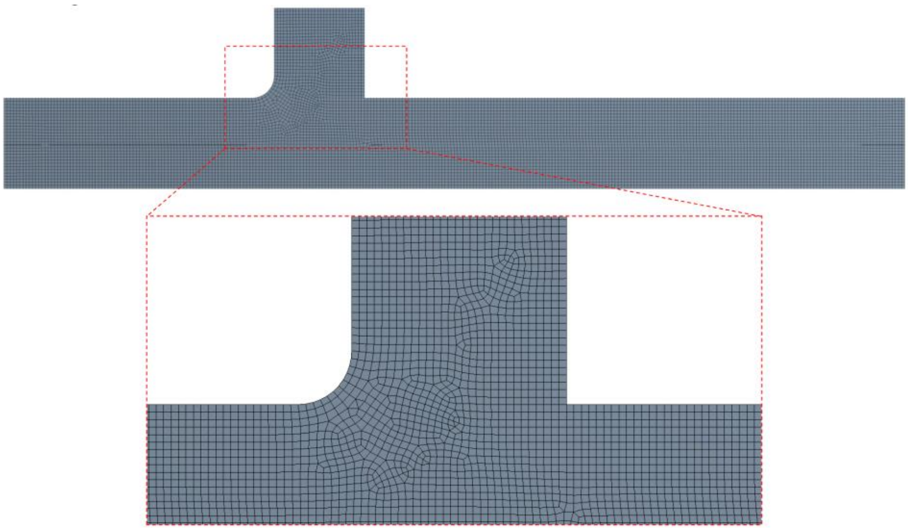

Figure 3. The full domain is discretized in 9,149 small elements. A detail of the cavity with rounded corner is in the bottom figure.

where the curvature κ of the interface water-oil is obtained by $\kappa = \nabla \cdot \left(\frac{\nabla \alpha_o}{|\nabla \alpha_o|}\right)$.

Initial and boundary conditions:

In the two-dimensional problem presented at Cartesian coordinates, there are five unknowns $[u,\ v,\ p,\ \alpha_w,\ \alpha_o]$ and five equations [Eqs. (3), (4-x), (4-y), (5), (6)]. For the solution, boundary conditions must be specified. These conditions are represented by letter (a) till letter (d) in Fig. 2 and means the following:

(a) At the entrance, the injected fluid (water) speed is prescribed as $V_w = 0.001$ m/s and is kept constant during all flow;
(b) At the exit plane, the pressure is zero;
(c) Fixed walls, which means that the no-slip and no-penetration conditions are applied;
(d) At the interface, the Eq. 9 is applied.

C. Numerical considerations

Discretization algorithms:

The system of governing equations is solved numerically with the VOF method (Hirt and Nichols, 1981). The appropriate choice of the discretization methods is an important step of the simulation process and is based on the papers of Santos *et al*. (2016) and Coelho *et al*. (2016). To the coupling pressure-velocity the PISO – Pressure-Implicit with Splitting of Operators is selected. The evaluation of gradients of the conserved properties is obtained applying the method Least Squares Cell-Based. The model selected to interpolate the pressure is the PRESTO! – Pressure Staggering Option. When it comes to the momentum equation and volumetric fraction of the fluid, the models used are, respectively, QUICK – Quadratic Upwind Implicit Differencing Convective Kinematics and CICSAM – Compressive Interface Capturing Scheme for Arbitrary Meshes.

Mesh refinement:

Three levels of mesh refinement with unstructured elements are tested (3,118 elements, 9,149 elements and 15,141 elements). After comparisons in performance to represent the average volumetric fraction of oil, the mesh with 9,149 elements, orthogonal quality of 87.88% and an aspect ratio of 2.08, was selected (Fig. 3).

Choice of the timestep:

The choice of the timestep, Δt, is accomplished according to the recommendation of Bohacek (2010), which was also discussed at Coelho *et al.* (2016) and Santos *et al*. (2016). Three different conditions must be verified.

The first one is the Courant–Friedrichs–Lewy condition (CFL), that results in convective terms for an average flow velocity $u = V_w$. Yet, it is also a function of the Courant number Co and the size Δx of the representative mesh element in the spatial discretization, resulting in $\Delta t_{CFL} = \frac{Co\Delta x}{u}$.

The second restrictive condition includes the influence of the interfacial tension σ_{wo} and the density of the displacing fluid ρ_w. It is the capillary timestep Δt_B proposed by Brackbill *et al.* (1992) $\Delta t_B = \left(\frac{\rho_w \Delta x^3}{2\pi\sigma_{wo}}\right)^{0.5}$.

Finally, the condition to biphasic flow with low and medium viscosity μ_w proposed by Galusinski and Vigneaux (2008) $\Delta t_V = \frac{\mu_w \Delta x}{\sigma_{wo}}$.

As a solution for this problem, considering the Courant number $Co = 0.25$ and the element velocity equal to the entrance velocity, the three obtained timesteps are $\Delta t_{CFL} = 0.025$ s, $\Delta t_B = 0.0046$ s and $\Delta t_V = 0.0135$ s. The Brackbill condition requires the smaller timestep to ensure the stability of the solution process, and that is assumed in this paper. The final time to study the retained oil fraction must be sufficiently long so it does not influence the results of the displacement process, being $t_D = 2.3$ for water-wet and intermediate wettability conditions, and $t_D = 11.5$ when oil is the wetting fluid.

D. Dimensionless parameters

The most important dimensionless parameters in the process of water-oil displacement can be divided into three categories: physical, numerical and geometrical, and are the following.

Table 1. Studied cases in this paper. The changes are in the curvature radius of the corner r_D, in the wettability θ_{wo} and dimensionless time t_D. The others parameters $\mu_R = 1$, $Ca = 1$, $Re = 1$, $Bo = 132.43$ and $Co = 0.131$ were kept constants.

Case	r_D %	θ_{wo}	t_D
1	5	90°	2.3
2	10	90°	11.5
3	25	90°	2.3
4	10	180°	11.5
5	10	0°	11.5

Capillarity number (Ca):
$Ca = \frac{\mu_w V_w}{\sigma_{wo}}$, that refers to the importance of viscous forces in relation to capillarity forces. The term σ_{wo} represents the surface or interfacial tension.

Reynolds number (Re):
$Re = \frac{\rho_w V_w h}{\mu_w}$, compares the importance of the inertia forces in relation to the viscous forces. Low values of Reynolds number indicate laminar flows and high values characterize a turbulent performance.

Bond number (Bo)*:*
$Bo = \frac{\Delta\rho g h^2}{\sigma_{wo}}$, also known as Eötvös Number, defines the relation of the gravitational forces with the interfacial forces. $\Delta\rho$ represents the difference of specific mass between oil and water, g is the gravity acceleration and h is the vertical distance.

Viscosity ratio (μ_R):
$\mu_R = \frac{\mu_o}{\mu_w}$, is the rate between the oil viscosity that is present at the domain and the viscosity of the water to be injected.

Courant number (Co):
$Co = V_w \frac{\Delta t}{\Delta x}$, is a criterion that aims to ensure the numerical stability in the transients problems solutions with the explicit approach, and must not be bigger than 1. V_w is the average velocity of the injected fluid; Δt is the time step and Δx the size of a representative element of the mesh.

Dimensionless time (t_D):
$t_D = \frac{V_w t}{\phi L}$, where the simulation time, t, is in seconds, the fluid drains to an average speed (equal to entrance speed), V_w, through of the canal of length $L = 10h$, with porosity ϕ. Replacing the known values and to unitary porosity, the dimensionless time is $t_D = 0.1t$.

Dimensionless curvature radius (r_D):
$r_D = \frac{r}{h}$, being r the corner radius (Fig. 2), that is used to improve the representation of the problem.

The described methodology has been applied previously by Pena *et al*. (2014), Romero and Fejoli (2015b), Coelho *et al*. (2016), Santos *et al*. (2016), and Rigatto and Romero (2018) to solve biphasic problems in the microscale.

E. Studied cases

To carry out the simulations, 25,000 time steps are used with 0.0046 seconds each. The average time of each simulation was approximately 16 hours of continuous use in an Intel® Core™ i3, 3GB of RAM computer.

The dimensionless parameters that characterize the phenomenon studied are presented in Table 1 for the five scenarios analyzed.

III. RESULTS AND DISCUSSIONS

A. General behavior

The bi-dimensional process of oil displacement by water is detailed in nine stages in Fig. 4 for case 2 with $r_D = 10\%$ and intermediate wettability $\theta_{wo} = 90°$. At the very beginning, as the streamlines become parallel, the flow develops in approximately 1 mm, from the entrance of the channel. As the fluid velocity is higher in the centerline and null in the walls, the water-oil interface is curved and tends to move more easily through the central region of the channel, leaving an oil film of approximately 0.17 mm ($0.17h$) attached to the walls. For this reason, the distance between the most advanced part of the interface and the contact line with the wall tends to increase with time (Fig. 4a, b, c, d, and e). Rigatto and Romero (2018) obtained similar response.

The microcavity creates a distortion of the streamlines since the presence of an abrupt expansion in one side of the domain makes the flow asymmetric and allows vertical movement of the fluid. As a result, it tends to expand in a typical phenomenon of die swell (Batchelor *et al*., 1973). Although it is not expressive, it can be observed counterclockwise recirculations in the cavity due to the transfer of momentum of the displacement fluid (water) to the displaced fluid (oil) that remains retained. The almost symmetric recirculation, while the interface is in the upper side of the cavity, gains asymmetry as the interface reaches the cavity and is displaced in the outlet channel direction.

The contact line moves along the corner curvature until it stabilizes in the initial vertical section of the left wall of the cavity, and this occurs at $t_D = 0.644$ (Fig. 4d). The contact line is apparently fixed, because in this region the recirculation of the oil and the movement of the injected fluid (water) are in the same direction. This creates a region where the flow is predominantly extensional. In the other corner of the cavity with null radius, the oil flow becomes thinner as it gets closer to the exit plane (Fig. 4e). As the injection is maintained, the unbalance of viscous and capillary forces in the sharp corner causes a rupture in the oil flow (Fig. 4f). For this point on (Figs. 4g and 4h) the process aims to remove the oil from the outlet channel. The simulation is sustained up to $t_D = 2.3$ in order to ensure that the volume retained in the cavity effectively represents residual oil saturation (Fig. 4i).

The first conclusion is that a great part of the oil in the cavity gets trapped. The oil that was removed is almost entirely from the one that had filled the channel. The sequence of nine images illustrates the negative impact of pore presence on the effectiveness of the extractive process. Although only one pore has been considered, the analysis can be extended to more than one, and the phenomenon will be repeated, with its own particularities.

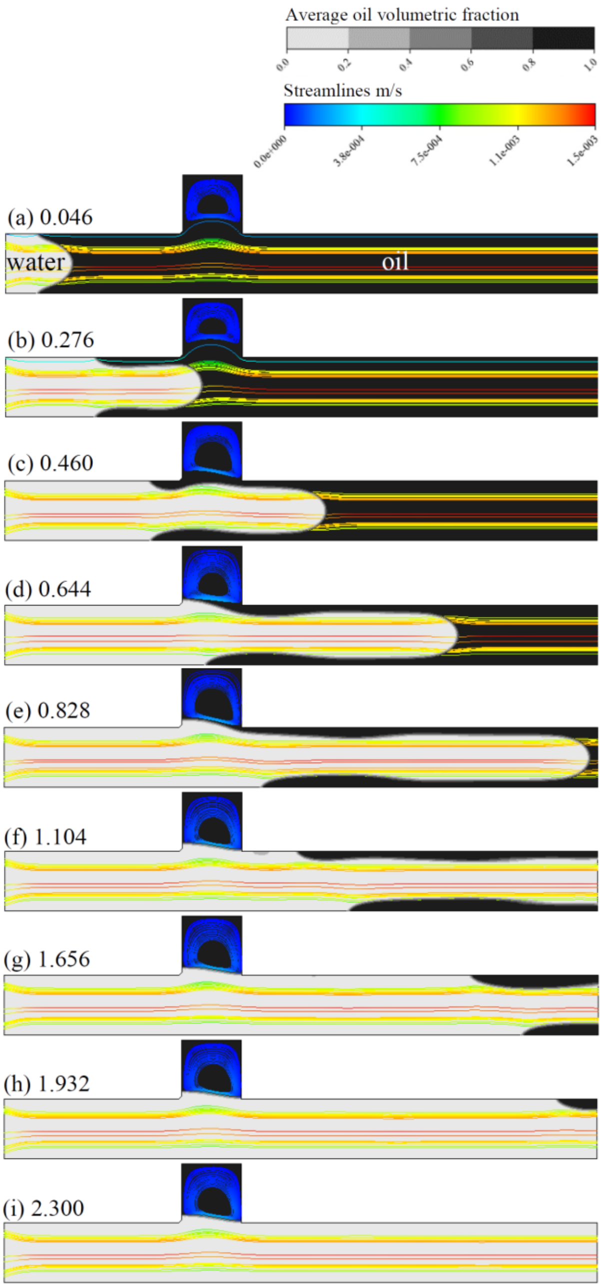

Figure 4. Qualitative behavior of the water-oil displacement process changing with (dimensionless) time t_D. At the end, oil remains trapped in the square cavity, which is an evidence of the inefficiency of the oil recovery process.

The use of different values of the dimensionless parameters, such as the capillarity number, will cause changes in these responses (Coelho *et al.*, 2016).

The qualitative response shown and discussed in Fig. 4 is presented quantitatively in Fig. 5 using the average volume fraction of oil $\bar{\alpha}_o(t)$ obtained from Eq. 10, which is similar to Eq. 1, for several time instants.

$$\bar{\alpha}_o(t) = \frac{\sum_{i=1}^{n} \alpha_{oi} vol_i}{\sum_{i=1}^{n} vol_i}, \quad (10)$$

vol_i is the volume of each element i of the discrete domain with $n = 9{,}149$ elements, α_{oi} is the oil volumetric fraction in each element, which is represented by α_o in previous sections.

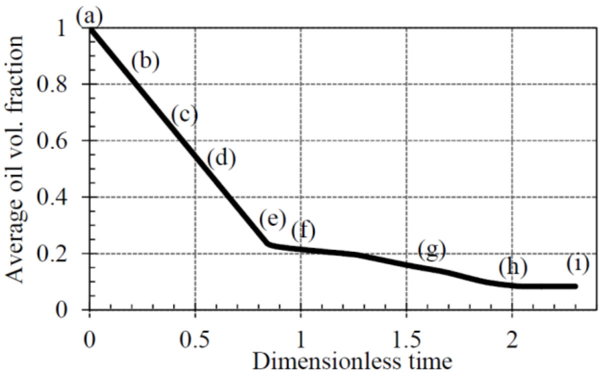

Figure 5. Reduction of the average fraction of oil retained in the microcavity at several time instants. Letters (a) to (i) are positions related with Fig. 4. From (h) to (i), the horizontal line represents the residual oil saturation, which is the limit of oil mobilization of the method. Additional oil only could be displaced with, for example, reduction of capillary effects or another EOR approach. The last dimensionless time is $t_D = 2.30$.

Figure 5 shows that the amount of oil decreases with the time of water injection, however, the behavior follows three well-defined regions. First, a linear region in which the recovery of oil is proportional to the time of injection, positions (a) to (e) in Fig. 5. A second region, in which proportionality no longer occurs and less oil is mobilized. The transition occurs at a critical time $t_D^{c1} \approx 0.844$, shortly after the configuration of Fig. 4(e). This change in response occurs when the water-oil interface reaches the outlet plane, which is the breakthrough (BT), and after that water is produced together with the oil. That implies that the displaced amount of oil decreases and the volume of water increases. This observation is supported by Fig. 4(f) at $t_D = 1.104$, in which the most advanced part of the interface is already out of the domain, and the time corresponds to the non-linear transition region of Fig. 5. The third region is a practically constant baseline that identifies the fraction of oil retained $\bar{\alpha}_{o\_final}$ in the porous medium and that can no longer be moved. It is the lower limit of the interval $\bar{\alpha}_{o\_final} \leq \bar{\alpha}_o(t) \leq 1$, point (h) in Fig. 5, which remains constant and is no longer modified by the continuous injection of water. The momentum transferred by the injected water is not sufficient to overcome the capillary and viscous forces that cause oil retention. This region starts at the critical time $t_D^{c2} \approx 2.05$ and extends to the end of the simulation in $t_D = 2.3$ for this case, point (i) in Fig. 5.

B. Radius of curvature influence

The efficiency of the oil mobilization process for the three radii of curvature of the corner (Table 1) is best visualized by plotting the final average volumetric fraction of oil ($\bar{\alpha}_{o\_final}$) at the end of simulation, according to Fig. 6. For the analyzed conditions, the increase of the dimensionless curvature radius results in a proportional reduction of the oil volume fraction. This linear trend is valid for specific fluid proprieties and cavity dimensions.

The variation with time of this parameter was discussed in Rigatto and Romero (2018).

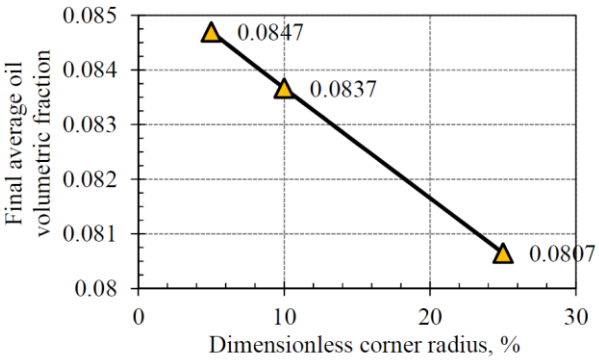

Figure 6. Influence of the curvature radius of the corner in the residual oil saturation.

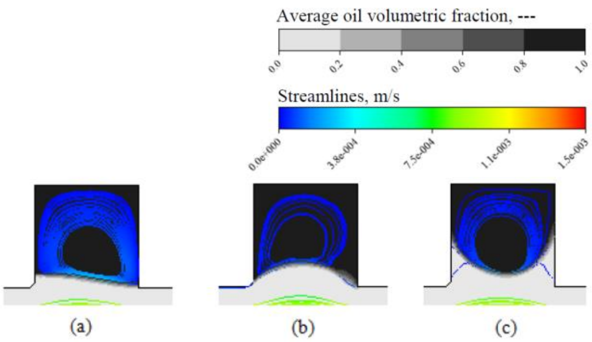

Figure 7. The wettability influence in the oil volumetric fraction for (a) intermediate wettability $\theta_{wo} = 90°$, (b) oil as wetting fluid $\theta_{wo} = 180°$, and (c) water as wetting fluid, $\theta_{wo} = 0°$ in $t_D = 11.50$.

C. Influence of wettability

Oil reservoirs are complex structures frequently formed by different types of sediment and filled with fluids whose properties can change from one point to another. This combination may cause the rock to be wettable to water or oil, or to have a neutral wettability (Abdallah *et al.*, 2007). Understanding the influence of this parameter is important mainly during the oil extraction process. The influence of wettability is evaluated through the contact angle θ_{wo}. In this study, three values of this parameter are considered: 90° (neutral wettability), 180° (wetting oil) and 0° (wetting water). To make these comparisons, the simulations were conducted five times longer than the previous cases. The radius of the corner is kept constant at $r_D = 10\%$, and the volumetric fraction fields of the oil and water are presented at the end of the transient process, $t_D = 11.50$, according to Fig. 7.

The interface takes different forms according to wettability. This behavior is much more evident in the cavity and has a significant impact on the process. For neutral wettability, $\theta_{wo} = 90°$, the interface is almost a line that forms a right angle in the solid walls and presents some asymmetry due to the greater advancement on the side of the rounded corner, Fig. 7a. When the wetting oil system is considered, $\theta_{wo} = 180°$, the interface becomes concave almost symmetrical with the contact lines practically attached to the corners, although the center of the recirculations tends to move closer to the rounded corner, Fig. 7b. In this condition, the difficulty to displace the oil

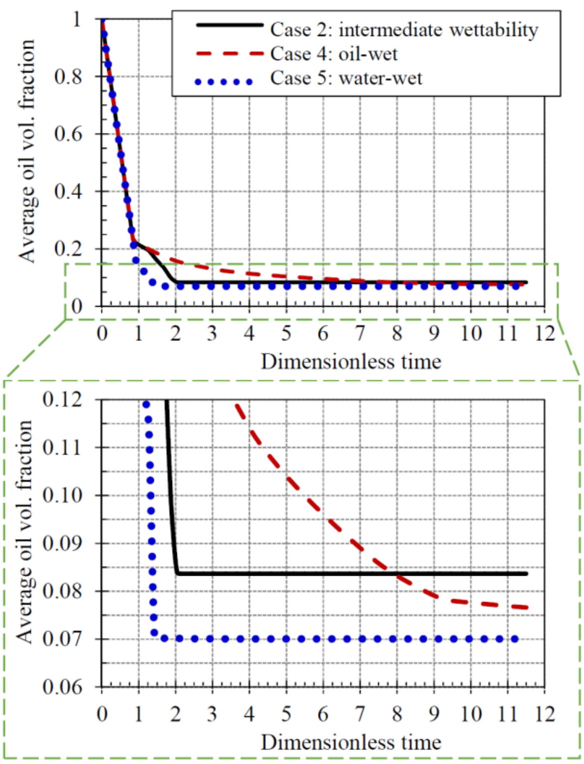

Figure 8. Influence of the wettability in the average volumetric fraction of the oil. The last dimensionless time is $t_D = 11.50$, five times longer than the previous cases (response presented in Fig. 5, for example).

is greater, being prejudicial to the extraction process efficiency. When water is the wetting fluid, $\theta_{wo} = 0°$, the interface takes the convex form, Fig. 7c. The invasion is more expressive, resulting in an improvement in the removal of the oil.

The behavior of the average volumetric fraction of oil with time for the three wettabilities are compared in Fig. 8. The upper figure shows the full (vertical) scale, where the three characteristic regions are evident: linear oil reduction, transition region and constant response region. A detail of the transition and constant regions is better visualized in the bottom figure.

The best performance in the oil displacement process is for the water wetting system ($\theta_{wo} = 0°$, case 5), where a small amount of oil remains trapped at the pore. In addition, the oil trapped at the cavity achieves its smaller value in a short time ($t_D = 1.43$) and then remains constant until the end. When the angle of adherence is 90° (case 2) the oil is recovered is also fast, in t_D =2 it becomes constant but with less oil being mobilized than the previous case.

When the concavity of the water-oil interface is convex, because of the oil wettability ($\theta_{wo} = 180°$, case 4), the reduction of oil saturation is very slow. There are a resistance to oil displacement by water due to the adherence of the oil to the solid surface. Only at t_D =~10, seven times bigger than the water-wet system, the curve becomes constant until the end of the simulation in t_D =11.5. At t_D≈8 there is an alternation in the performance for the situations with intermediate wettability and

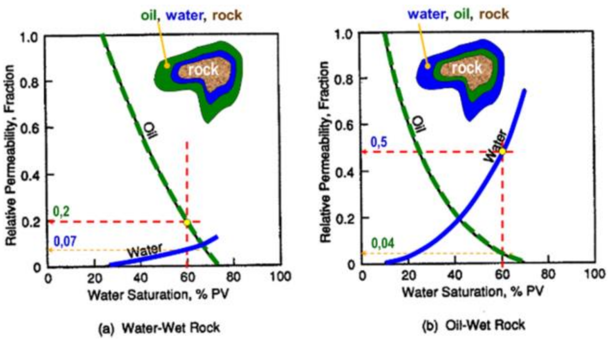

Figure 9. Influence of the wettability in the effective permeability in a two-phase water-oil system (adapted from: Romero, 2019).

oilwetting, that can only be seen for long times. The final efficiency is intermediate between the water-wet and neutral wettability systems.

The discussed results are in accordance with the curves of effective permeability affected by wettability in a water-oil system (Fig. 9).

Since the stabilization of the average oil volume fraction occurs, the recovery of additional oil of the microcavity is no longer possible with the recovery method employed.

What should be the response for different viscosity ratios? From macroscopic point of view, more viscous oil results in unfavorable mobility ratios and, as a consequence, less efficient displacement process (Green and Willhite, 1998). Is this behavior possible to capture at the microscale? Our research is going in that direction.

IV. CONCLUSIONS

Considering the displacement of Newtonians, immiscible and incompressible fluids, in the laminar and transient flow regime, in which the fluid is located inside a microcavity, it was analyzed the effects of the radius of the corner of the microcavity and the wettability of the system in the average volumetric fraction of the oil. The solution of the two-phase problem was based on the VOF approach and the analysis of the obtained results allows conclude the following:

a) As observed in Figs. 5 and 8, the oil displacement process by water can be classified obeying three different behaviors, keeping up with the oil volumetric fraction. The first is a linear region where the displaced volume is equal to the injected volume. The second one is a transition region where the amount of displaced fluid decreases gradually. And a third region where no additional volume of oil is displaced.
b) At the end of the process, a certain quantity of oil will remain trapped in the microcavity, showing the inefficiency of the conventional recovery by water injection. The trapped oil is the residual oil, that is the result of the predominance of the capillarity forces over the viscous forces that promote the displacement.
c) The process becomes more efficient with the increase of micropore curvature radius. That occurs because sharp corners with curvature radius next to zero make the contact line displacement difficult. For higher radius, the contact line slips more easily, favoring the invasion of the region that contains the oil and, consequently, its displacement.
d) The wettability has a direct effect on the amount of oil displaced and in the required computational cost:
   - Being the water the wetting fluid, a greater amount of oil is mobilized with relatively little computational efforts;
   - Being the system wetting oil, the oil mobilization is much slower, requiring longer times to achieve the constant baseline (five times bigger in this case), and it is also less efficient.
e) There is an alternation in the performance for the situations with intermediate wettability and oil-wetting, that can only be seen for long times.

Other parameters, as the viscosity ratio, capillarity number and geometry of the pore must be changed in future works in order to expand the problem comprehension.

ACKNOWLEDGEMENTS

The authors would like to thank FAPES for the financial support through “Edital FAPES 21/2018 – Universal”, document number 159/2019. Also thanks to SPE UFES Student Chapter for granting the access of OnePetro platform <onepetro.org>.

REFERENCES

Abdallah, W., Buckley, J.S., Carnegie, A., Edwards, J., Herold, B., Fordham, E., Graue, A., Habashy, T., Seleznev, N., Signer, C., Hussain, H., Montaron, B. and Ziauddin, M., (2007) Fundamentals of wettability. *Oilfield Review*. Summer, 44 – 61,

ANSYS Inc. (2013) *ANSYS Fluent Theory Guide*. Release 15.0.

Batchelor, J., Berry, J.P. and Horsfall, F. (1973) Die swell in elastic and viscous fluids. *Polymer*. **14**, 297-299.

Bohacek, J. (2010) Surface tension model for high viscosity ratios implemented in VOF Model. *23th Annual Conference on Liquid Atomization and Spray Systems.* Brno, 1-8.

Brackbill, J., Kothe, D. and Zemach, C. (1992) A continuum method for modeling surface tension. *Journal of Computational Physics.* **100**, 335-354.

Coelho, J.K., Pena, M.D. and Romero, O.J. (2016) Porescale modeling of oil mobilization trapped in a square cavity. *IEEE Latin America Transactions*. **14**, 1800–1807.

Galusinski, C. and Vigneaux, P. (2008) On stability condition for bifluid flows with surface tension: application to microfluidics. *Journal of Computational Physics,* **227**, 6140-6164.

Gibbs, J.W. (1961) *Scientific papers of J. Willard Gibbs*, Volume I Thermodynamics. Dover publications. New York.

Green, D.W. and Willhite, G.P. (1998) *Enhanced oil recovery*. AIME Society of Petroleum Engineers. Richardson, Texas.

Guidi, M.C. and Romero, O.J. (2018) Numerical simulation of surfactant flooding in petroleum reservoirs. *IEEE Latin America Transactions*. **16**, 1700-1707.

Hirt, C.W. and Nichols, B.D. (1981) Volume of fluid (VOF) method for the dynamics of free boundaries. *Journal of Computational Physics*. **39**, 201–225.

Kamyabi, A., Ramazani, A.S.A. and Kamyabib, M.M. (2013) Effects of viscoelastic polymer solutions on the oil extraction from dead ends. *Scientia Iranica*. **20**, 1912-1920.

Kamyabi, A., Ramazani, A.S.A. and Kamyabi, M.M. (2015) Surfactant effects on the efficiency of oil sweeping from the dead ends: numerical simulation and experimental investigation. *Chemical Engineering Research and Design*. **94**, 173-181.

Martins, J.R., Ribeiro, D.C., Pereira, F.A.R., Ribeiro, M.C. and Romero, O.J. (2020) Heat dissipation of the Electrical Submersible Pump (ESP) installed in a subsea skid. *Oil & Gas Science and Technology-Rev*. *IFP Energies nouvelles*. **75**, 13.

Muggeridge, A., Cockin, A., Webb, K., Frampton, H., Collins, I., Moulds, T. and Salino, P. (2014) Recovery rates, enhanced oil recovery and technological limits. *Philosophical Transactions of The Royal Society. Series A, Mathematical, Physical, and Engineering Sciences*. **372**, 20120320.

Oliver, J.F., Huh, C. and Mason, S.G. (1977) Resistance to spreading of liquids by sharp edges. *Journal of Colloid and Interface Science*, **59**, 568-581.

Pena, M.D., Romero, O.J. and Ribeiro, D.C. (2014) Mobilização de óleo retido em microcavidades mediante injeção de fluidos não-newtonianos inelásticos. *Latin American Journal of Energy Research*. **1**, 30-38.

Pereira, I.B., Ribeiro, D.C. and Romero, O.J. (2017) Three-Dimensional Modelling of Heat Transfer in Wellbore During Steam Injection Process. *IEEE Latin America Transactions*. **15**, 690-697.

Rigatto, S.F. and Romero, O.J. (2018) Deslocamento de óleo por água em um microcanal com cavidade de quinas arredondadas. *Holos*. **8**, 19-34.

Romero, O.J (2019) *Enhanced oil recovery*. Course. Federal University of Espirito Santo.

Romero, O.J. and Fejoli, R.F. (2015a) Fluxo de uma gota de óleo em um canal reto e com garganta. *Revista Iberoamericana de Ingeniería Mecánica*. **19**, 71-81.

Romero, O.J. and Fejoli, R.F. (2015b) Foam injection as a mechanism of mobility control in reservoir rocks. *Revista Internacional de Métodos Numéricos para Cálculo y Diseño en Ingeniería*. **31**, 218-227.

Romero, O.J., Scriven, L.E. and Carvalho, M.S. (2006) Effect of curvature of coating die edges on the pinning of contact line. *AIChe Journal*, **52**, 447-455.

Santos, K.B., Romero, O.J., Meneguelo, A.P. and Ribeiro, D.C. (2016) A numerical investigation of immiscible water-oil displacement in simplified porous media. *IEEE Latin America Transactions*. **14**, 2175–2183.

Soares, I.L. and Romero, O.J. (2019) Pore-scale modeling of oil displacement by pulsed water injection. *Ingeniería e Investigación*. submitted.

Wei, B., Zerón, L.R. and Rodrigue, D. (2014) Oil displacement mechanisms of viscoelastic polymers in enhanced oil recovery (EOR): a review. *Journal of Petroleum Exploration and Production Technology*. **4**, 113–121.

Yin, H., Wang, D. and Zhong, H. (2006) Study flow behaviors of viscoelastic polymer solution in micropore with dead end. *SPE Annual Technical Conference and Exhibition*, San Antonio, Texas, USA Paper 101950.

Zitha, P., Felder, R., Zornes, D., Brown, K. and Mohanty, K. (2019) *Increasing Hydrocarbon Recovery Factors*. Available in: <https://www.spe.org/industry/increasing-hydrocarbon-recovery-factors.php>, accessed on June 3.

Received October 27, 2019
Sent to Subject Editor March 5, 2020
Accepted September 1, 2020
Recommended by Subject Editor Walter Tuckart